Scripta Materialia 128 (2017) 83–86

Contents lists available at ScienceDirect

Scripta Materialia

journal homepage: www.elsevier.com/locate/scriptamat

Regular Article

Correcting for contact area changes in nanoindentation using surface acoustic waves

Christian E. Beck [a], Felix Hofmann [b], Jeffrey K. Eliason [c,1], Alexei. A. Maznev [c], Keith A Nelson [c], David E.J. Armstrong [a,*]

[a] Department of Materials, University of Oxford, Parks Road Oxford, OX1 3PH, UK
[b] Department of Engineering Science, University of Oxford, Parks Road, Oxford, OX1 3PJ, UK
[c] Department of Chemistry, Massachusetts Institute of Technology, 77 Massachusetts Avenue, Cambridge, MA 02139, USA

ARTICLE INFO

Article history:
Received 30 August 2016
Received in revised form 27 September 2016
Accepted 28 September 2016
Available online 15 October 2016

Keywords:
Nanoindentation
Pile-up
Ion implantation
Irradiation
Surface acoustic waves

ABSTRACT

Nanoindentation is extensively used to quantify nano-scale mechanical behaviour. A widely-used assumption is that a well-defined, material-independent relationship exists between the indentation depth and indenter contact area. Here we demonstrate that this assumption is violated by ion-implanted tungsten, where pileup around the indenter tip leads to substantial changes in contact area. Using high accuracy surface acoustic wave measurements of elastic modulus, we are able to correct for this effect. Importantly we demonstrate that a priori knowledge of elastic properties can be readily used to compensate for pileup effects in nanoindentation without the need for any further measurements.

1. Main body

Most nanoindentation analysis methods assume that surface pileup or sink-in plays a negligible role in determining contact area for the calculation of hardness and modulus [1–3]. However, whilst applicable to a small number of materials, this is far from universally true. Methods for determining the *actual* contact area include post-test measurements using transmission electron microscopy (TEM) replicas [4], scanning electron microscopy (SEM) [5], or atomic force microscopy (AFM) [6]. However post-test examination has major restrictions. It is time consuming and must be carried out on individual indents that may not be representative. More importantly the examination is inherently carried out on the unloaded indentation impression, unlikely to represent the true contact area due to elastic recovery on unloading. This effect is particularly significant for small indents in elastically stiff and mechanically hard samples [7]. Nanoindentation performed inside the SEM can provide observations of changes in pile up morphology [8], however, with a single static viewpoint, it does not allow determination of contact area.

Here we propose an alternative approach that utilises simultaneous modulus and hardness measurements enabled by the Continuous Stiffness Measurement (CSM) method used on many nanoindentation systems [3]. If the modulus can be measured independently, changes in contact area due to pileup can be corrected for, allowing a substantially more accurate determination of indentation hardness.

Ion implantation is extensively used to mimic irradiation damage in nuclear reactor materials [9–12]. The ability to accurately probe mechanical properties of these modified layers is highly desirable. Bulk mechanical tests on heavy ion-implanted layers are not possible as the implanted layers are only a few microns thick due to limited ion penetration. Electron microscopy and atom probe tomography have been widely used to study the microstructural changes within these thin layers [13]. Their mechanical properties have been predominantly studied using nanoindentation to measure hardness changes. However the reliability of these measurements is questionable since even at low damage levels substantial variations in pileup morphology and hence contact area can occur. This has been observed for example in W-5 wt%Ta implanted with 2 MeV W^+ ions to damage level of 0.04 displacements per atom (dpa) [14], where pile up is significantly suppressed after implantation. Interestingly no changes in pileup morphology were observed in HT9 steel implanted with both helium-ions and protons [10]. Yet in Fe^+ implanted Fe-12 wt%Cr significant changes in pileup both as a function of indentation depth and indenter type have been reported after implantation [5]. However, the majority of nanoindentation studies on ion-implanted surfaces simply do not consider potential change in pile morphology and the effect they may have on the determined hardness and modulus values [15–17].

* Corresponding author.
E-mail address: david.armstrong@materials.ox.ac.uk (D.E.J. Armstrong).
[1] Present affiliation: Department of Chemical Engineering and Materials Science, University of Minnesota, 421 Washington Avenue SE, Minneapolis, MN 55455, USA.

http://dx.doi.org/10.1016/j.scriptamat.2016.09.037
1359-6462/

Our previous nanoindentation measurements on tungsten alloys showed a large apparent increase of both elastic modulus and hardness after ion implantation [14,18]. This is surprising since recent density functional theory calculations and surface acoustic wave measurements both indicate that the elastic modulus of tungsten is reduced by helium-ion implantation [19]. Eqs. (1) and (2) show that changes in contact area will affect the measurement of both hardness and elastic modulus, with pile-up resulting in an overestimate of both quantities and sink-in an underestimate. This suggests that the reported large increase in modulus *and* hardness [18] is likely to be due to an *underestimation* of the true contact area during indentation. By measuring the elastic modulus of the implanted layer using an independent technique, such as surface acoustic wave (SAW) measurements [19–21], a correction factor for the contact area can be calculated allowing a correct hardness value, accounting for the pile up, to be determined. Here we employ this new approach to determine the true hardness of a 2.5 μm thick He^+ implanted surface layer in a W-1 wt% Re alloy sample.

The W-1 wt% Re alloy was produced by arc-melting of elemental powders: 99.9% W, (Sigma Aldrich, USA) and 99.99% Re (AEE, USA), as described in [18]. The resulting ingot was sectioned into 1 mm thick slices and polished using a final colloidal silica polishing step to produce a high quality surface finish, the composition was verified using electron probe micro-analysis. Helium ion-Implantations were performed at 573 K at the National Ion Beam Centre, University of Surrey, UK. Multiple ion energies (from 0.05 MeV to1.8 MeV), were used to produce an approximately uniform helium concentration of 3110 ± 270 appm and corresponding damage of 0.24 ± 0.02 dpa within a 2.5 μm thick surface layer, for full implantation details see Beck et al. [18]. The calculated implantation profiles, estimated using the Stopping Range of Ion in Matter (SRIM) code [22] with a displacement energy of 68 eV, are shown in Fig. 1.

Nanoindentation was performed on an MTS NanoXp with a Berkovich diamond indenter tip. Calibration indents in fused silica, using the continuous stiffness measurement (CSM) technique [3] with a 45 Hz and 2 nm oscillation, were used to fit a polynomial expressing contact area, A(d), as a function of indenter displacement, d, into the surface. Hardness, H (d), and indentation modulus, E*(d), were then computed using Eqs. (1) and (2) respectively:

$$H(d) = \frac{P(d)}{A(d)}, \tag{1}$$

$$E^*(d) = \frac{dP}{dd}(d)\frac{1}{2}\frac{\sqrt{\pi}}{\sqrt{A(d)}}, \tag{2}$$

where P(d) is the applied load as a function of displacement.

Indents were made to displacements of (a) 2000 nm and (b) 250 nm. Deep indents (a) allowed identification of the indent depths at which behaviour is dominated by the implanted layer. Shallow indents (b) served to study pileup morphology at these depths. Fig. 2a shows modulus vs indenter displacement and (Fig. 2b solid markers) hardness vs indenter displacement data. Hardness shows the expected behaviour with a small size effect seen in the unimplanted sample, and significant hardening after implantation, similar in magnitude to that seen in pure tungsten implanted with helium to similar doses [23]. In the unimplanted sample modulus varies little with indentation depth and the recovered value of 400 GPa is consistent with the literature value of Young's modulus for pure tungsten [24–26]. The implanted sample shows a significant increase in modulus to a maximum value of 475 GPa at indentation depths between 100 nm and 350 nm. At the maximum indentation depth of 2000 nm there is still an increases in modulus of 5% to a value of 420 GPa. This dramatic increase in elastic modulus is inconsistent with previous atomistic calculations and experimental measurements [19,27].

AFM micrographs of the 250 nm deep indents were recorded using a Digital Instruments Dimension 3100 microscope in contact mode (nominal tip radius 10 nm) and SEM micrographs were collected using a Zeiss Auriga FEG FIB/SEM (Fig. 3). In the unimplanted sample a small amount of pile-up is observed around the indent (Fig. 3a). The implanted sample

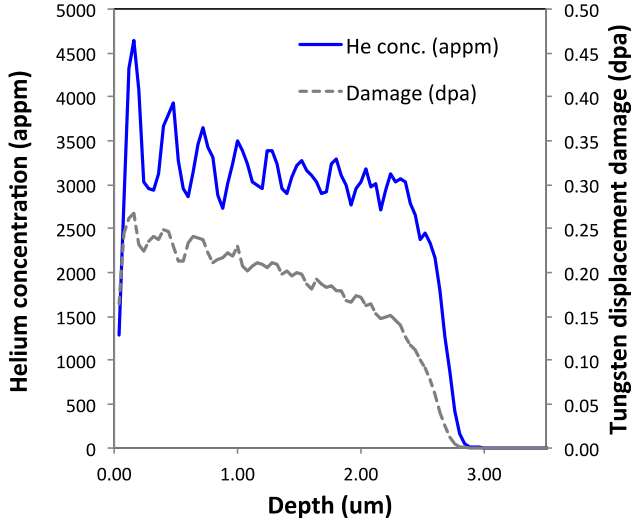

Fig. 1. Helium ion concentration and displacement damage caused by the ion implantation as calculated using the SRIM code.

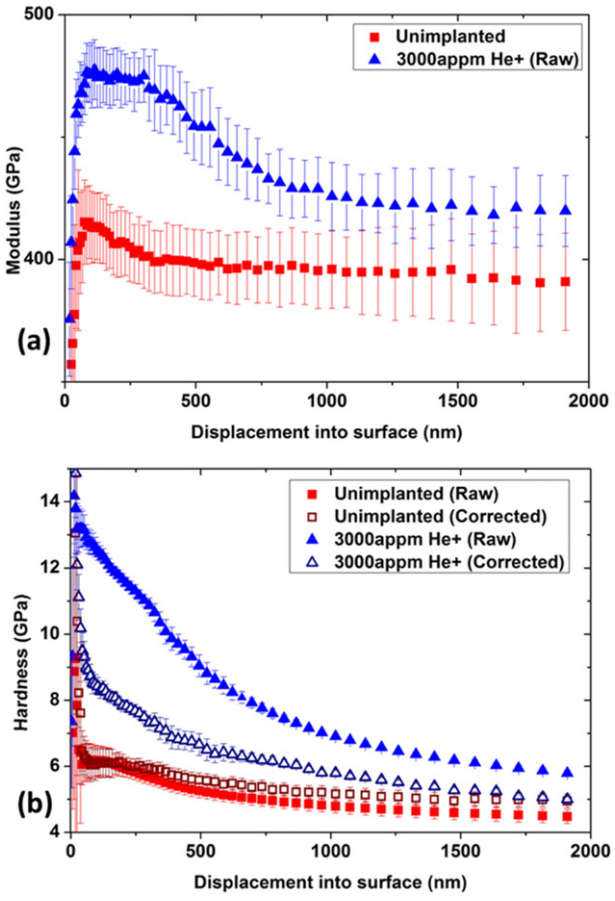

Fig. 2. (a) Indentation modulus as a function of depth for unimplanted (red) and He^+ implanted (blue) W-1 wt% Re. (b) Raw indentation hardness for unimplanted and implanted W-1 wt% Re (closed symbols). True indentation hardness values corrected using SAW measured modulus values (open symbols).

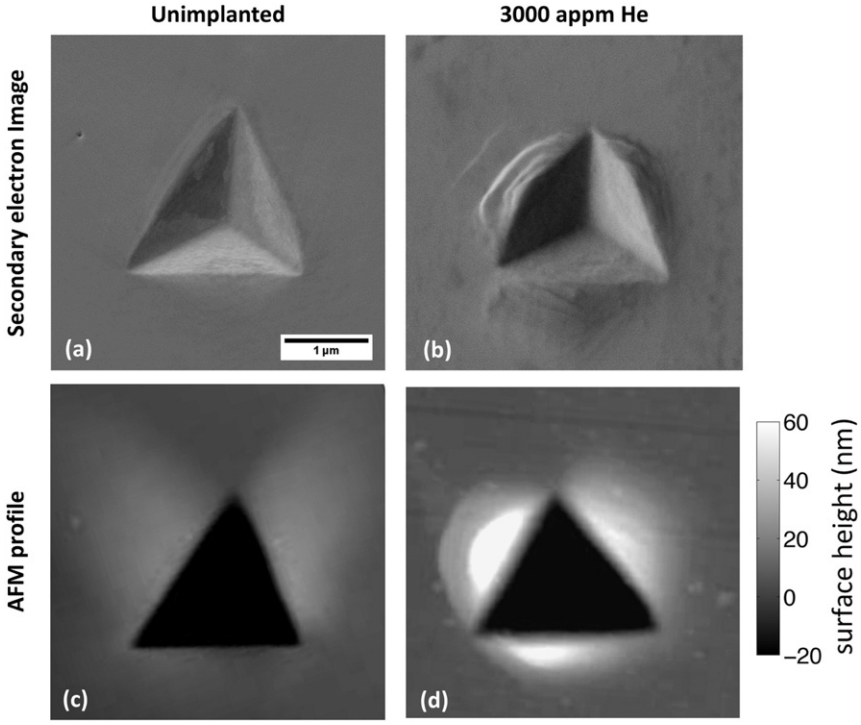

Fig. 3. Micrographs of 250 nm deep indents. (a) and (b) surface normal SEM images of indents in the unimplanted and He $^{+}$ implanted sample respectively. (c) and (d) AFM topography maps of indents in the unimplanted and He^{+} implanted sample respectively. The scale bar is the same for all images.

shows a substantial increase in pile-up as well as evidence of slip localisation (Fig. 3b and d). The representative nature of these observation was verified by scanning 8 further indents on each sample. Due to the small size of these indents and the inability to observe the degree of pile up in the "as loaded" state, a contact area correction by the post mortem analysis of the pile up was not attempted.

Transient grating (TG) laser measurements were used to measure the elastic properties of the ion-implanted surface layer. A detailed description of the technique is provided elsewhere [20]. Briefly, two short excitation laser pulses (515 nm wavelength, 60 ps pulse duration, 1.75 μJ pulse energy, ~500 μm spot diameter) were crossed on the sample. Interference of the light generates a spatially sinusoidal interference pattern with a wavelength of $\lambda = 2.75$ μm. Rapid thermal expansion of the sample, following absorption of the light, launches two counter-propagating surface acoustic waves (SAWs). These are detected using diffraction of a quasi-continuous probe beam (532 nm wavelength, 300 μm spot diameter, 10 mW power) from the surface modulations induced by the SAWs. The diffracted beam was measured using a fast avalanche photo-diode (1 GHz bandwidth) and time traces were recorded with an oscilloscope. By Fourier transforming the resulting signal, SAW frequency, f, and hence the Rayleigh wave velocity, c_r, were determined. For a SAW wavelength λ, c_r is dominated by a layer of thickness ~ $\lambda/2$ [19]. For the excitation wavelength of $\lambda = 2.74$ μm used here this is significantly less than the implanted layer thickness of ~3 μm.

For an elastically isotropic medium (tungsten at room temperature is very close to elastically isotropic [24–26]), the Rayleigh velocity, c_r, is approximately given by:

$$c_r = f\lambda \approx (0.874 + 0.196\nu - 0.043\nu - 0.055\nu^3)\sqrt{\frac{E}{2(1+\nu)\rho}} \quad (3)$$

where ρ is density and the maximum error compared to the exact solution is less than 0.45% [28]. Rearranging Eq. (3) for Young modulus, E, and using $\rho = 19{,}260\ \mathrm{kgm}^{-3}$ and $\nu = 0.2796$ [28], the Young moduli for the unimplanted and helium-implanted tungsten alloy samples (which are close to elastically isotropic) were found to be 411.3 ± 0.4 GPa and 393.5 ± 2.2 GPa respectively. These values are in good agreement with predictions from density functional theory [19].

For the unimplanted sample E_{SAW} agrees well with E_{ind}. However for the helium-implanted sample E_{ind} is significantly overestimated due to the large pile up (Fig. 3). To correct for this, a correction coefficient, C_{cor}, was calculated, as defined by Eq. (4). Considering Eqs. (1) and (2), C_{cor} can then be used to determine the true indentation hardness, H_c, from the apparent indentation hardness, H (Eq. (5)).

$$C_{cor} = \left(\frac{E_{ind}}{E_{SAW}}\right)^2, \quad (4)$$

$$H_C = H_I C_{cor} \quad (5)$$

Fig. 2b shows the resulting, true indentation hardness for the He^{+} implanted material (open symbols). Comparing the true indentation hardness to the apparent indentation hardness, shows that neglecting the effect of pileup leads to a substantial overestimate of hardness; 3.7 GPa (48%) at 250 nm indentation depth and 0.7 GPa (14%) for 2000 nm deep indents. We also note that at larger depth (2000 nm) the true indentation hardness curves for both the unimplanted and implanted sample converge to the same value (5 GPa). This confirms, as expected, that for these larger indents plastic behaviour is dominated by the response of the underlying unimplanted material.

In summary our results demonstrate that pileup behaviour and hence indentation contact area can change substantially as a result of ion-implantation. By performing an independent measurement of the elastic modulus of the implanted material, pile up can be corrected for, allowing an accurate measurement of the hardness of the implanted material. Interestingly pileup behaviour is not only modified by ion implantation. For example residual stresses can significantly alter the pile up formed in otherwise identical materials, leading to inaccurate measurements of modulus and hardness [29]. Our approach of using a priori information about elastic properties (ideally independently verified by

experiment or modelling) to correct for pileup effects is applicable to all such cases and allows true hardness values to be measured.

Acknowledgements

We are grateful to N. Peng for carrying out the ion implantation at Surrey National Ion Beam Centre, UK. DEJA acknowledges support from the Royal Academy of Engineering through a Research Fellowship. FH acknowledges funding from the John Fell fund (122/643) and the Royal Society (RG130308). The SAW measurements at MIT were supported by NSF grant no. CHE-1111557. This work was part-funded by the United Kingdom Engineering and Physical Sciences Research Council via programme grant EP/H018921/1. The data in this paper is available on Oxford Research Archive [30].

References

[1] J.S. Field, M.V. Swain, J. Mater. Res. 8 (1993) 297–306.
[2] S.V. Hainsworth, H.W. Chandler, T.F. Page, J. Mater. Res. 11 (1996) 1987–1995.
[3] W.C. Oliver, G.M. Pharr, J. Mater. Res. 7 (1992) 1564–1583.
[4] J.B. Pethica, R. Hutchings, W.C. Oliver, Philos. Mag. A 48 (1983) 593–606.
[5] C.D. Hardie, S.G. Roberts, A.J. Bushby, J. Nucl. Mater. 462 (2015) 391–401.
[6] N. Moharrami, S.J. Bull, Thin Solid Films 572 (2014) 189–199.
[7] L. Charleux, V. Keryvin, M. Nivard, J.P. Guin, J.C. Sangleboeuf, Y. Yokoyama, Acta Mater. 70 (2014) 249–258.
[8] J.M. Wheeler, V. Maier, K. Durst, M. Goken, J. Michler, Mater. Sci. Eng. A 585 (2013) 108–113.
[9] D.E.J. Armstrong, C.D. Hardie, J.S.K.L. Gibson, A.J. Bushby, P.D. Edmondson, S.G. Roberts, J. Nucl. Mater. 462 (2015) 374–381.
[10] P. Hosemann, C. Vieh, R.R. Greco, S. Kabra, J.A. Valdez, M.J. Cappiello, S.A. Maloy, J. Nucl. Mater. 389 (2009) 239–247.
[11] E.A. Marquis, R. Hu, T. Rousseau, J. Nucl. Mater. 413 (2011) 1–4.
[12] C. Heintze, F. Bergner, M. Hernandez-Mayoral, J. Nucl. Mater. 417 (2011) 980–983.
[13] P.D. Edmondson, A. London, A. Xu, D.E.J. Armstrong, S.G. Roberts, J. Nucl. Mater. 462 (2015) 369–373.
[14] D.E.J. Armstrong, A.J. Wilkinson, S.G. Roberts, Phys. Scr. T145 (2011) 014076.
[15] J.D. Hunn, E.H. Lee, T.S. Byun, L.K. Mansur, J. Nucl. Mater. 282 (2000) 131–136.
[16] D.E.J. Armstrong, X. Yi, E.A. Marquis, S.G. Roberts, J. Nucl. Mater. 432 (2013) 428–436.
[17] Z.J. Huang, A. Harris, S.A. Maloy, P. Hosemann, J. Nucl. Mater. 451 (2014) 162–167.
[18] C.E. Beck, S.G. Roberts, P.D. Edmondson, D.E.J. Armstrong, MRS Online Proc. Libr. 1514 (2013) 99–104.
[19] F. Hofmann, D. Nguyen-Manh, M.R. Gilbert, C.E. Beck, J.K. Eliason, A.A. Maznev, W. Liu, D.E.J. Armstrong, K.A. Nelson, S.L. Dudarev, Acta Mater. 89 (2015) 352–363.
[20] J.A. Johnson, Department of Chemistry, Massachusetts Institute of Technology, 2011.
[21] J. Goossens, P. Leclaire, X.D. Xu, C. Glorieux, L. Martinez, A. Sola, C. Siligardi, V. Cannillo, T. Van der Donck, J.P. Celis, Journal of Applied Physics, 102, 2007.
[22] J.F. Ziegler, M.D. Ziegler, J.P. Biersack, Nucl. Inst. Methods Phys. Res. B 268 (2010) 1818–1823.
[23] D.E.J. Armstrong, P.D. Edmondson, S.G. Roberts, Appl. Phys. Lett. 102 (2013).
[24] G. Simmons, H. Wang, Single Crystal Elastic Constants and Calculated Aggregate Properties: A Handbook, 2d ed. M.I.T. Press, Cambridge, Mass., 1971
[25] D.I. Bolef, J. Deklerk, J. Appl. Phys. 33 (1962) 2311-&.
[26] R. Lowrie, A.M. Gonas, J. Appl. Phys. 38 (1967) 4505-&.
[27] D.R. Muss, J.R. Townsend, J. Appl. Phys. 33 (1962) 1804-&.
[28] M. Rahman, T. Michelitsch, Wave Motion 43 (2006) 272–276.
[29] G.M. Pharr, T.Y. Tsui, A. Bolshakov, W.C. Oliver, Mater. Res. Soc. Symp. Proc. 338 (1994) 127–134.
[30] Correcting for Contact Area Changes in Nanoindentation using Surface Acoustic Waves - Data. http://dx.doi.org/10.5287/bodleian:DOBvDrv0w